Simulink Computed Torque Control of a Novel 15-DOF Anthropomorphic Robotic Fingers

Deepak Bharadwaj[#], Roushan Kumar

Department of Mechanical Engineering, School of Engineering, University of Petroleum and Energy Studies, Dehradun, India

[#]Corresponding Author: *Deepak Bharadwaj, Email: dbharadwaj@ddn.upes.ac.in*

Abstract

Joint control is the prominent issue observed during finger interaction with the environment. Internal collision of finger movement during grasping of the object occurs while picking the object. This research work focuses on the placement of joint motor, so that finger collision can be avoided. Due to compact size and advancement of sensing and actuation, the flat plate motor was directly mounted between the finger joint. Touch sensors were placed on the surfaces of the finger. A simple master-slave control was adopted for the finger joint motion control. A smooth operation of grasping was observed during finger interaction.

Keywords: Collision, Control architecture, Finger interaction, Computed torque control

1. INTRODUCTION

Finger gripper controlling is a tedious task. The main problem arises due to actuator size. Placing of larger size actuator between the fingers is not possible and also for mobile applications, there is a chance of collision [1]. Earlier design work on the pulley system, four-bar chain mechanism, and gear mechanism. The conventional mechanism is limited to the workspace for the finger during grasping the object [2],[3]. The conventional mechanism has no flexibility to deal with the unknown shape and size of the object. Due to the larger size of the mechanism and more weight of the actuator, grasping is not done properly. With the advancement of flat plate EC motors, such type of problems can be minimized. Flat plate motor sizes vary from 10 mm thickness to 50mm thickness and the diameter of rotor size varies from 2mm-20mm. The flat plate EC motor has an inbuilt quadrature encoder. The current trends in robotics research shifted to the placement of the plate motor [4]. These motors can easily be fitted between the joints. This research work focuses on the placing of the plate motor between the joints.

Controlling of 15_DOF finger joint is also a very tough task. A simple master and slave control architecture was used for the finger gripper control. The advantage of master and slave type control architecture did not put the controller to do computation. The Master is controlling the finger position and the slave is controlling each joint position. The feedback was sent to the master controller and the master controller the correction if any deviation happens while the interaction of the finger gripper during the grasping of the object.

2. MECHANICAL DESIGN

A 3-D model was prepared on the Solid work plate form. The dimension was kept approximately to the human finger dimension. The model consists of 15 joints. Each finger has three joints [5]. Each joint was connected with one flat plate motor. To simplify the control, one common shaft is connected to a flat plate motor. One motor is controlling the three joints simultaneously. The schematic details of the finger gripper are shown in figure 1.

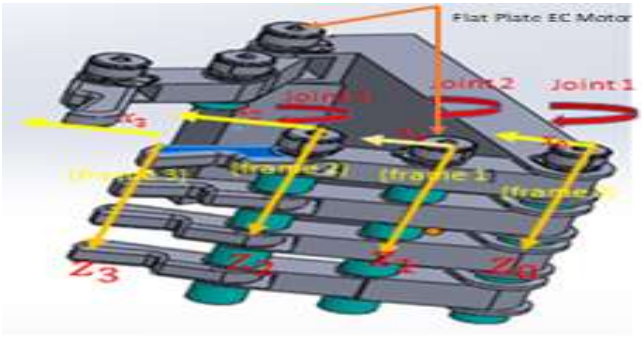

Figure 1. 3-D Modelling of Finger Gripper

3. CONTROL ARCHITECTURE

In its environment, a finger gripper completes the designated activities, which fall into two categories: contact-type tasks and non-contact-type jobs [6]. Actuators that impart a force or a torque to the links in order to move them are what power and drive each individual joint of a finger manipulator [7]. The manipulator control system gives the actuator commands necessary to move the manipulator and produce the desired end effector motion [8]. These instructions are based on the control set points produced from the collection of joint torque time histories that the trajectory planner collected. To obtain precise motion, the control system might be given back with the actual joint and/or end effector positions and their derivatives. The control system may use input on the actual joint locations and velocities, as indicated by the dotted lines for the feedback. The parameter q , $\dot{q}$ and $\ddot{q}$ and τ and so on. Joints cannot move independently, and a complex control algorithm will be required. A master control system that synchronises and controls n-joints makes up the usual robot control architecture for an n-DOF manipulator [9]. Sending "set point" instructions to each of the joint controllers is the responsibility of this master control. The set point data is used by the n-joint controllers to instruct the joint actuator to move the joint. The joint controller may employ feedback to the master controller. The Multi-Input –Multi-output (MIMO), nonlinear dynamics model of the n-DOF manipulator becomes

$$\tau = M(q)\ddot{q} + H(q,\dot{q}) + \dot{G}(q) \qquad (1)$$

Fig. 2. Manipulator control system

Because this controller is based on a more accurate dynamic model of a manipulator, it provides better trajectory performances than linear controllers do. The controller discussed here employs the computed torque control law to modify the system effectively decouple and linearize it [10]. The computed torque control scheme also comprises two portions- a model-based and a servo portion [11],[12]. The schematic diagram of a manipulator control system is shown in figure 2. The model-based portion defines the nx1 vector of control torques τ using a structure. Where $\dot{\tau}$ is the nx1 torque vector specified by the servoposition.

$\tau = M(q)\dot{\tau} + H(q,\dot{q}) + \dot{G}(q)$ (2)

$\dot{\tau} = \ddot{q}$ (3)

By using nonlinear feedback of the real locations and velocities of joints, the model-based portion efficiently linearizes and decouples the dynamics of the system. Figure 3 illustrates the schematic depiction of this nonlinear control strategy.

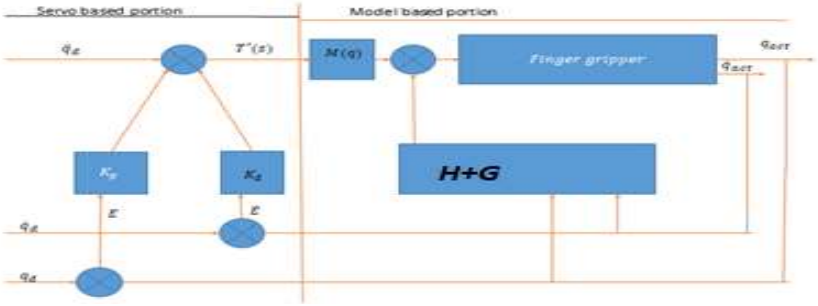

Fig .3. Control architecture of computed control

The control law of the servo portion based on the nx1 vectors E and $\dot{E}$ of the servo errors in joint positions and velocities, respectively. The servo portion of the computed torque control scheme is, therefore, defined as

$E(t) = q_d(t) - q(t)$ *(4)*

And $E(t) = \dot{q}_d(t) - \dot{q}(t)$ *(5)*

Where $q$and q_d denote the nx1 vectors of actual and desired joint positions respectively. The servo portion of the computed torque control scheme is, therefore, defined as

$\dot{\tau} = \ddot{q}_d + K_d\dot{E} + \dot{K}_pE$ *(6)*

Where $K_p$and K_d are the nxn matrices of position and velocity gains, respectively. Usually $K_p$and K_d are chosen as diagonal matrices with constant gains. This serves to decouple the error dynamics of the individual joints [13],[14]. The model of error behavior or error dynamics is obtained from

$\ddot{q} = \ddot{q}_d + K_d\dot{E} + \dot{K}_pE$ *(7)*

or with $\ddot{E} = \ddot{q}_d - \ddot{q}$ *(8)*

$\ddot{E} + K_d\dot{E} + \dot{K}_pE = 0$ *(9)*

This shows that the error dynamics of a closed–loop system are specified by a second-order linear error equation. This vector equation is decoupled if K_p and K_d are diagonal matrices with constant gain. Hence the error equation could be written on a joint-by-joint basis. For joint i the error equation is

$\ddot{e}_i + K_{di}\dot{e}_i + K_{pi}e_i = 0$ *(10)*

Where $K_{pi}$and K_{di} are the position and velocity gains, respectively, for joint i. For the critically damped performance of joints, the relationship between $K_{pi}$and K_{di} is obtained in equation i.e

$K_{di} = 2\sqrt{K_{pi}}$ *(11)*

3.1 Gain Parameter

The equation specifies the methodology for setting the control gains K_p and K_d.A direct consequence of the control law, equation, is that the servo error at any instant of time is zero provided there is no initial error and the computation time for the computer is zero, i.e the actuator torque is computed as a continuous function of time [15],[16]. In reality, the time taken to compute the servo error, the PD law control gains, and to command a new value of torque, is nonzero and is known as the cycle time. This

is the resulting command torque $\dot{\tau}_a$ is a staircase function and the servo error is non-zero at the beginning of each cycle [17]-[19]. The controller will reduce this nonzero servo error to zero during each cycle [20-23]. Based on these parameters the control gain K_p and K_d are computed as listed in Table1.

Table 1. Control gain values of K_p and K_d

Gain/Joint	K_p	K_d
Joint 1	12	8
Joint 2	10	6
Joint 3	8	4

Hence the actual trajectory tracked will be close to, but not the same as desired trajectory. Apart from a damping ratio of unity, another factor that constrains the selection of control gains is the flexibility of links, which are assumed to be rigid bodies in the development of the joint model. The unmodeled structural flexibility of the link and other mechanical elements produces resonance at frequencies other than natural frequency. Because these structural flexibilities have been ignored, the controller must be designed so as not to excite these unmoulded resonances. The lowest unmoulded resonance, which corresponds to the maximum value of the effective inertia seen by the actuator,I_{max} has a resonance frequency

$$\omega_{res} = \omega_o \sqrt{\frac{I_o}{I_{max}}} \qquad (12)$$

where ω_o is the structural frequency when the effective inertia is I_o. To prevent exciting these structural oscillations and also ensure structural stability, the controller's natural frequency ω_n must be limited to $0.5\omega_{res}$.i,e

$$\omega_n \leq 0.5\omega_{res} \text{ and } K_p \leq (0.5\omega_o)^2 \frac{I_o}{I_{max}} \qquad (13)$$

4. RESULTS AND DISCUSSION

The simulation was carried out for the planned trajectory of the different joints. The cubic spline polynomial equation has been used for trajectory planning. The boundary condition is applied at the start and end of the trajectory.

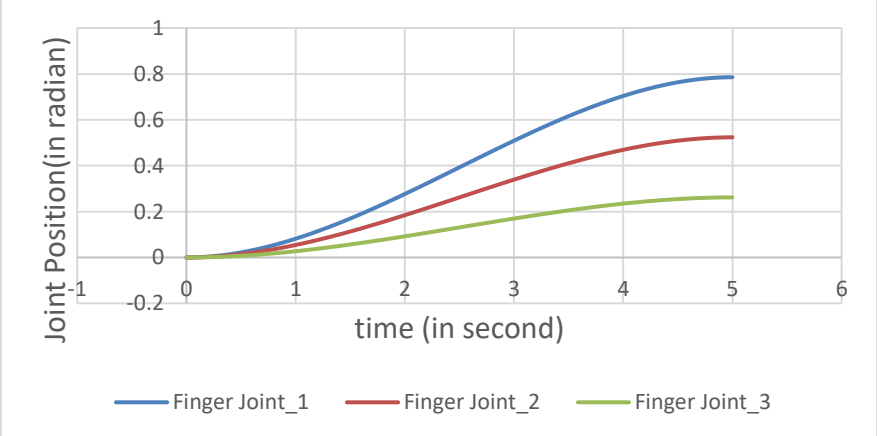

Fig .4. Planned trajectory

Initially, the joint position and velocity are zero. Hence there is no jerk coming at the start and the end of the motion. The cubic spline polynomial equation creates the smooth trajectory of the joint movement. The finger joint speed up for 2.5 seconds of travel and the next half comes to speed down. The simulation was carried out for 5 seconds for the minimum and maximum values of the individual joints. Figure 4 shows the finger joint position with respect to time. Coriolis and centrifugal force resist the motion of the finger joint to reach the desired position. The proportional gain and derivative gain were taken [12; 10; 8] and [8; 6:4] based on the values obtained from the equation. Tuning of the gain can increase the joint position reached near the grasped object. A deviation can be observed in figure 5 between the planned and actual trajectory of the finger

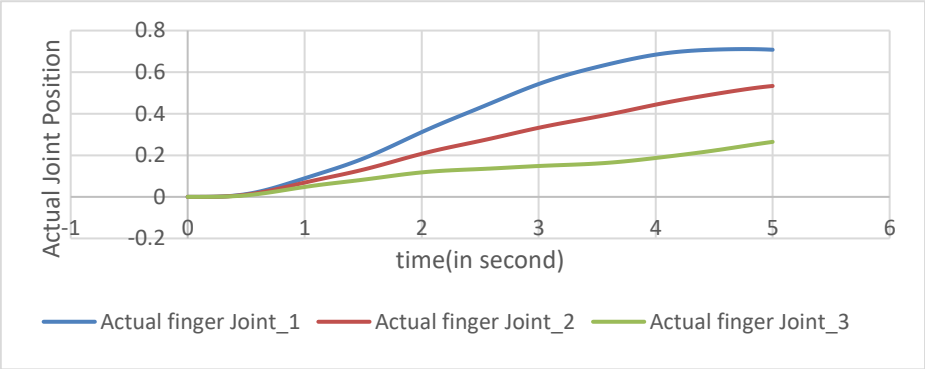

Fig .5. Actual trajectory of finger joint

5. CONCLUSION

A new finger gripper design was considered for the grasping of the unknown shape and size of the object in the unknown environment. The 3-point touch of the finger during an interaction makes the robotic finger gripper flexible. A large workspace was observed compared to the conventional design. The master-slave approach of the control system makes the system very easy to manipulate the object.

References

[1] M. Liu, L. Hao, W. Zhang, and Z. Zhao, "A novel design of shape-memory alloy-based soft robotic gripper with variable stiffness," *Int. J. Adv. Robot. Syst.*, vol. 17, no. 1, pp. 1–12, 2020, doi: 10.1177/1729881420907813.

[2] R. Kumar, N. J. Ahuja, M. Saxena, and A. Kumar, "Modelling and Simulation of Object Detection in Automotive Power Window," Indian J. Sci. Technol., 2016;9 (43) doi: 10.17485/ijst/2016/v9i43/104393.

[3] M. Honarpardaz, M. Tarkian, J. Ölvander, and X. Feng, "Finger design automation for industrial robot grippers: A review," *Rob. Auton. Syst.*, vol. 87, pp. 104–119, 2017, doi: 10.1016/j.robot.2016.10.003.

[4] R. Kumar, Divyanshu, and A. Kumar, "Nature Based Self-Learning Mechanism and Simulation of Automatic Control Smart Hybrid Antilock Braking System," Wirel. Pers. Commun., 2021; 116(4); 3291–3308 doi: 10.1007/s11277-020-07853-7.

[5] M. Kaur and W. S. Kim, "Toward a Smart Compliant Robotic Gripper Equipped with 3D-Designed Cellular Fingers," *Advanced Intelligent Systems*, vol. 1, no. 3. p. 1970032, 2019, doi: 10.1002/aisy.201970032.

[6] D. Bharadwaj and M. Prateek, "Kinematics and dynamics of lower body of autonomous humanoid Biped Robot," *Int. J. Innov. Technol. Explor. Eng.*, vol. 8, no. 4, 2019.

[7] D. Gan *et al.*, "Actuation-Coordinated Mobile Parallel Robots With Hybrid Mobile and Manipulation Functions," *J. Mech. Robot.*, vol. 14, no. 4, Mar. 2022, doi: 10.1115/1.4053821.

[8] M. Takizawa, S. Kudoh, and T. Suehiro, “Design and implementation of a multi-DOF hand and basic motions for rope-knotting tasks,” *Adv. Robot.*, vol. 36, no. 10, pp. 463–473, 2022, doi: 10.1080/01691864.2022.2070866.
[9] Kumar, R., Gupta, N., Bharadwaj, D., Dutt, D., & Joshi, A. (2022). Design and development of electronic clutch control unit for manual transmission. Materials Today: Proceedings. https://doi.org/10.1016/j.matpr.2022.08.470
[10] D. Bharadwaj, M. Prateek, and R. Sharma, “Development of reinforcement control algorithm of lower body of autonomous humanoid robot,” *Int. J. Recent Technol. Eng.*, vol. 8, no. 1, 2019.
[11] Kumar, R., Gupta, M. K., Kumar, A., Sharma, P., & Deorari, R. (2022). Analysis of electronic clutch control unit for manual transmission vehicle oriented toward safety. Materials Today: Proceedings. https://doi.org/10.1016/j.matpr.2022.08.473
[12] S. Nicosia and A. TORNAMBÈ, “Use of asymptotic observers in the parameter estimation of robotic manipulators having elastic joints,” *Adv. Robot.*, vol. 5, no. 4, pp. 349–376, 1990, doi: 10.1163/156855391X00250.
[13] R. Kumar, K. Bansal, A. Kumar, J. Yadav, M. K. Gupta, and V. K. Singh, “Renewable energy adoption: Design, development, and assessment of solar tree for the mountainous region,” Int. J. Energy Res. 2021; 1–17 doi: 10.1002/er.7197.
[14] H. Tourajizadeh and S. Manteghi, “Design and optimal control of dual-stage Stewart platform using Feedback-Linearized Quadratic Regulator,” *Adv. Robot.*, vol. 30, no. 20, pp. 1305–1321, 2016, doi: 10.1080/01691864.2016.1212735.
[15] R. Kumar, R. K. Pachauri, P. Badoni, D. Bharadwaj, U. Mittal, and A. Bisht, “Investigation on parallel hybrid electric bicycle along with issuer management system for mountainous region,” J. Clean. Prod., 2022; 362:132430, doi: 10.1016/j.jclepro.2022.132430.
[16] Kumar, R., Kumar, A., Gupta, M. K., Yadav, J., & Jain, A. (2022). Solar tree-based water pumping for assured irrigation in sustainable Indian agriculture environment. Sustainable Production and Consumption, 33, 15-27, doi.org/10.1016/j.spc.2022.06.013.
[17] R. Kumar, N. J. Ahuja, M. Saxena, and A. Kumar, “Automotive Power Window Communication with DTC Algorithm and Hardware-in-the Loop Testing,” Wirel. Pers. Commun., 2020;114 (4): 3351–3366 doi: 10.1007/s11277-020-07535-4.
[18] C. S. Meera, S. Sunny, R. Singh, P. S. Sairam, R. Kumar, and J. Emannuel, “Automated precise liquid transferring system,” 2014:1-6 doi: 10.1109/IICPE.2014.7115831.
[19] Kurre, S.K., Yadav, J., Thakur, S. (2022). Comparative Study of the Rear and Rear Side Impact on a Roll Cage Using FEM. In: Singh, M.K., Gautam, R.K. (eds) Recent Trends in Design, Materials and Manufacturing. Lecture Notes in Mechanical Engineering. Springer, Singapore. https://doi.org/10.1007/978-981-16-4083-4_37.
[20] Yadav, J., Kurre, S.K., Thakur, S. (2022). FEM-Based Impact Analysis of Roll Cage of an All-Terrain Vehicle. In: Singh, M.K., Gautam, R.K. (eds) Recent Trends in Design, Materials and Manufacturing. Lecture Notes in Mechanical Engineering. Springer, Singapore. https://doi.org/10.1007/978-981-16-4083-4_17.
[21] Yadav, Jitendra, Santosh Kumar Kurre, and Shubham Thakur. "Estimation of the dynamic response of roll cage under impact loading by modeling and simulation." Materials Today: Proceedings 50 (2022): 2181-2188. https://doi.org/10.1016/j.matpr.2021.09.445
[22] Yadav, Jitendra, et al. "Nonlinear dynamics of controlled release mechanism under boundary friction." Results in Engineering 11 (2021): https://doi.org/10.1016/j.rineng.2021.100265
[23] Dravid Shriram, Jitendra Yadav, and Santosh Kumar Kurre. "Comparison of loosening behavior of bolted joints using plain and spring washers with full-threaded and plain shank bolts." Mechanics Based Design of Structures and Machines (2021): 1-19. https://doi.org/10.1080/15397734.2021.2008258.